

High harmonic generation spectra of aligned benzene in circular polarized laser field

Petra Žďánská and Vitali Averbukh

Department of Chemistry, Technion—Israel Institute of Technology, Haifa 32000, Israel

Nimrod Moiseyev^{a)}

Department of Chemistry, Technion—Israel Institute of Technology, Haifa 32000, Israel

and Minerva Center for Nonlinear Physics of Complex Systems, Technion—Israel Institute of Technology, Haifa 32000, Israel

(Received 29 October 2002; accepted 19 February 2003)

We present model calculations of high-order harmonic generation in benzene, aligned in the polarization plane of circular polarized laser field. The resonance states of the system are obtained using complex scaling Floquet approach (i.e., within non-Hermitian quantum mechanics) combined with (t, t') time propagation method. Our results show that the photo-induced dynamics of the model benzene molecule at the laser wavelength of 800 nm is dominated by a single long-lived resonance state up to the intensity of about 90 TW cm^{-2} . The high-order harmonics emitted by the system obey the selection rules derived in [Phys. Rev. Lett. **80**, 3743 (1998)] on the basis of the dynamical symmetry of the system, namely the emitted harmonics possess the frequencies $(6 \pm 1)\omega, (12 \pm 1)\omega, \dots$, where ω is the incident laser frequency. These symmetry-allowed harmonics are found to be the dominant ones in the spectrum also when the laser polarization deviates from the “ideal” circular one by about 5%. The nonlinear response of the model benzene molecule is found to originate mainly from the field-induced transitions between the bound states, in accordance with the earlier analytical theory. The cut-off position in the calculated high-order harmonic generation spectra depends linearly on the field strength in the studied intensity interval. Our numerical calculations reveal the enhancements of particular high-order harmonics in the plateau region of the spectrum at certain field intensities. We show that these enhancements occur under conditions of avoided crossing of two or several resonance quasi-energies in the complex energy plane. © 2003 American Institute of Physics. [DOI: 10.1063/1.1566737]

I. INTRODUCTION

High-order harmonic generation (HHG) by molecular gases interacting with strong linear polarized laser fields has been studied experimentally since mid-nineties.^{1–4} In the majority of these experiments diatomic, e.g., O_2 or N_2 , or other small molecular species were used. One of the main questions asked by the researchers was: “Do molecules behave as atoms, or are there additional effects induced by molecular structure?”³ However, the molecular HHG spectra were found to be generally similar to the atomic ones. In particular, there has been no indication that the mechanism of the generation of high-order harmonics by molecules is different from the well-known three-step mechanism of atomic HHG due to Corkum and Kulander.^{5,6} This mechanism based on the recollision of the ionized electron with the core explains the cutoff in atomic HHG spectra occurring at the photon energy of $E_{\text{ion}} + 3.2U_p$, where E_{ion} and U_p are the ionization energy of the atom and the ponderomotive energy of the ionized electron, respectively. Several theoretical works (see, e.g., Refs. 7 and 8) predict that dissociating diatomic and linear triatomic molecules with large internuclear separations are capable of producing high-order harmonics with energies far beyond the atomic HHG cutoff.

These ideas, though, still await their experimental realization (see Ref. 9 for the very recent experiment on HHG by dissociating iodine).

The experiments with medium-size organic molecules, such as butane, butadiene, benzene, cyclohexane, and naphthalene,^{10–13} have already revealed several specific features of molecular HHG. For example, the length of the laser pulse was found to be the key parameter defining whether it is the parent molecule or its dissociation products that are responsible for the HHG process. The drop in the intensities of the high-order harmonics emitted by organic molecules with increasing ellipticity of the incident field was found to be smaller than in the atomic case.¹³ This weaker ellipticity dependence was attributed by the authors to the larger cross section for the recollision of the ionized electron with the molecular ion.

The investigation of the dependence of HHG in molecular gases on the orientation of the molecules could reveal more of the distinctive features of molecular HHG. The experimental studies of this kind have become feasible since the molecular alignment in gas phase was achieved by the application of nonresonant laser pulses.¹⁴ The molecular orientation dependence of the HHG spectra was the subject of two theoretical works.^{15,16} The authors used two-center zero-range potential¹⁵ and soft Coulomb potential¹⁶ models

^{a)}Electronic mail: nimrod@tx.technion.ac.il

to calculate the single-molecule response to the high-intensity field. However, their conclusions concerning the relative efficiency of HHG by molecules aligned parallel or perpendicular to the field polarization axis, were qualitatively different. Very recently, the HHG by the laser-aligned linear molecules has been investigated experimentally by Hay *et al.*¹⁷ In these experiments, the best alignment was achieved for CS₂ molecules. It has been found that the alignment of this species leads to more efficient HHG than the one observed in the gas of randomly oriented CS₂. But contrary to the earlier theoretical predictions,^{15,16} the HHG efficiency was found to be independent of the direction of the molecular alignment. This result is consistent with the proposition that the phase matching effects play a dominant role in the enhancement of HHG by molecular alignment.¹⁷

The difference between atomic and molecular HHG is predicted to be the most striking in the case of interaction with circular polarized laser field. For symmetry reasons, atoms interacting with circular polarized field do not generate harmonics of the incident radiation frequency. On the other hand, the interaction of aligned molecules possessing N th-order rotational symmetry with circular polarized field brings about HHG with unusual selection rule, as shown by Alon, Averbukh, and Moiseyev.¹⁸ If the molecular symmetry axis is aligned with the propagation direction of the laser field, the emitted high-order harmonic frequencies are $\Omega = \omega, (lN \pm 1)\omega, l = 1, 2, \dots$, where ω is the fundamental frequency. The $(lN + 1)$ th harmonics are polarized circularly as the incident field, while the $(lN - 1)$ th harmonics are polarized circularly in the opposite way. The $(lN \pm 1)$ selection rule is a result of the spatio-temporal or dynamical symmetry (DS) of the time-dependent Hamiltonian of the symmetric molecule in the laser field.¹⁹

Of course, symmetry arguments alone are not sufficient in order to predict the relative intensities of the symmetry-allowed harmonics. Dynamical considerations has to be involved in order to elucidate the mechanism of HHG by symmetric molecules interacting with circular polarized field and to predict the efficiency of the process. A simple model of HHG by the symmetric N -center molecules aligned in the plane of circular polarized field has been proposed in Ref. 20. The studied model is a generalization of the strong-field approximation of Lewenstein and co-workers²¹ to the case of N bound states forming the minimal-size basis for the representation of the symmetry of the problem. The transitions between the N bound states were described using "inverse" perturbation theory.²² This perturbational approach is based on the assumption that the energy differences between the bound states of the system are significantly smaller than the energy of the interaction of the system with the field, $E_{\text{int}} = \mu_{\text{tr}}E_0$, where μ_{tr} is a typical transition dipole moment between two bound states and E_0 is the field amplitude. It was found that the dominant contribution to the HHG spectrum of the model system comes from the bound-bound transitions. The cutoff was shown to be located at the maximal variation of the interaction energy, $n_{\text{cutoff}} = 2E_0\mu_{\text{tr}}/\hbar\omega$. Since the energy of the highest-order harmonic in the plateau is related to the maximal change in E_{int} , the HHG by the considered class of systems can be interpreted as a trans-

formation of the interaction energy into the energy of the emitted photons. Such a mechanism was proposed earlier for HHG by two-center systems.^{15,22} It is qualitatively different from the one responsible for the atomic HHG at linear polarization,^{5,6} where the cutoff scales quadratically with the field amplitude.

The analytical theory of Refs. 18 and 20 allows us to understand the basic features of selective HHG by symmetric cyclic molecules interacting with circular polarized field. However, it is not sufficient in order to draw quantitative conclusions concerning the intensities of the emitted high-order harmonics. The reason is that the simple model²⁰ does not take into account the depletion of the bound states population due to the ionization. Moreover, it uses an idealized Hückel structure of the lower-energy molecular bound states and does not take into account at all Rydberg states of the molecule. It is, therefore, desirable to verify the conclusions of Refs. 18 and 20 by numerical calculations of HHG spectra for a realistic model potential representing a symmetric molecule, e.g., benzene. Numerical studies of this kind were very helpful for understanding the dynamics of HHG by rare gases, see for example, Ref. 23. In the case of selective molecular HHG, the model numerical calculations are a necessary step on the way to experimental observation of the phenomenon.

Recently, Ceccherini and Bauer proposed a two-dimensional model potential for the study of HHG by benzene aligned in the polarization plane of the laser.²⁴ The authors studied the interaction of a single active electron initially confined by the model potential with short laser pulses. Taking into account the finite pulse duration made it possible to study the appearance of the side bands in the HHG spectra of the system (see also Ref. 25). The positions of these satellite lines are related to the ac Stark shifts of the molecular states in the laser field. Their intensities are determined by the nonadiabatic transitions between the quasi-energy states of the system during the pulse²⁶ and cannot be obtained from the Floquet analysis of the type of the one presented in Ref. 18. Nevertheless, the key questions concerning the selective HHG by benzene are still open for numerical analysis. For instance, the calculation of Ref. 24 does not provide a systematic study of the cut-off position in the numerical HHG spectra, nor does it contain an analysis of the relative importance of the bound-bound and bound-continuum transitions for the HHG process. Consequently, the results of Ceccherini and Bauer do not explain the mechanism of HHG by symmetric species interacting with circular polarized field. Another point worthy a systematic numerical analysis is the effect of the deviation of the field polarization from the "ideal" circular one on intensities of the DS-forbidden harmonics. The nonunity ellipticity of the projection of the electric field on the molecular plane can also result from the nonideal alignment of the molecule. The stability of the selection rules with respect to the ellipticity of the incident field has been studied in Ref. 18 qualitatively using perturbation theory for Floquet states and was illustrated by means of HHG spectra of a bound one-dimensional model. A quantitative analysis of the behavior of HHG spec-

tra of imperfectly oriented molecules requires the inclusion of the ionization effect.

In the present work we use the two-dimensional model proposed by Ceccherini and Bauer in order to study the mechanism of HHG by benzene molecule aligned in the polarization plane of the 800 nm laser. The model reproduces correctly the realistic benzene ionization potential, which allows us to consider quantitatively the influence of the ionization on benzene HHG spectra. The calculations are performed within the framework of Floquet theory, i.e., neglecting the finite pulse length. We use complex scaling technique^{27,28} combined with (t, t') time propagation method²⁹ in order to obtain the resonance and continuum quasi-energy solutions of the problem in the interval of field intensities. Our results show that the photo-induced dynamics of the model is dominated by a single long-lived resonance state up to the intensity of about 90 TW cm^{-2} . We study the intensity dependence of the HHG spectra of the system being described by the narrow resonance. We indeed find the linear dependence of the cut-off energy on the incident field strength, however, the proportionality factor is found to be larger than the one predicted for the N -level model of Ref. 20. The HHG spectra of the ionizing system are compared with those of the bound model in which only the field-induced transitions between twelve bound states of the model potential are allowed. The results of our numerical calculations support the conclusion of the earlier analytical work²⁰ concerning the dominant role of the bound-bound transitions in the selective HHG process at circular polarization.

We calculate the dependences of the high-order harmonics in the plateau region of the HHG spectrum of the model benzene on the intensity of the incident laser field. These intensity dependences are shown to be characterized by an almost periodic pattern of enhancements. We show that field-dependent avoided crossings of the resonance quasi-energies of the system in the complex energy plane are responsible for this effect (see Refs. 30–32 for the effect of the avoided crossings of this type on nonlinear phenomena). The enhancements predicted here for the molecular HHG spectra are analogical to the resonance enhancements of high-order harmonics observed in the atomic case.³³ Furthermore, we extend our numerical calculations to the case of nonunity ellipticity to analyze the behavior of the DS-allowed and DS-forbidden harmonics at nonideal laser polarization and/or nonideal molecular alignment. It turns out that at 5% deviation from the circular polarization of the incident field, the DS-based selection rules still hold to a good approximation.

The present paper is organized as follows: Section II contains the description of the numerical methods which are used in the present study to calculate resonance states and HHG spectrum of the benzene molecule in circular polarized laser field. Section III is devoted to the discussion of resonance lifetimes over a wide range of laser intensities, and the appearance of avoided crossings in the complex-energy plane for certain values of laser intensities. We show that the appearance of avoided crossings is accompanied by the enhancement of the ionization rate and HHG. Section IV presents HHG spectra of benzene in circular polarized laser field

over a wide range of laser intensities. Focus is on the dependence of the spectrum cutoff on the laser intensity, and the detailed structure of dependence of the HHG intensities on the laser intensity. Finally, the full range calculations of HHG spectra are compared with the HHG spectra of the bound twelve-state model to explain the mechanism of the process. In Sec. V we address the issue of stability of the dynamical selection rules with respect to the deviation from laser circular polarization and/or with respect to the imperfect molecular alignment. We present our conclusions in Sec. VI.

II. MODEL FOR BENZENE DRIVEN IN THE STRONG ELECTRO-MAGNETIC FIELD

A. Single active electron two-dimensional (2D) model

In the present work, the harmonic generation of benzene is studied within the single active electron approximation. The description of the system consisting of the planar benzene molecule which is aligned in-plane with the driving electric field requires at least a two-dimensional model. The two-dimensional potential for the active electron of aligned benzene has been proposed by Ceccherini and co-workers.^{24,25} Within this model, the driven electron can be ionized from one of the carbon atoms represented by six regularized “carbon” Coulomb wells distributed symmetrically on a ring. The potential of Ceccherini *et al.* reads

$$V(\rho, \phi) = -\frac{A}{\sqrt{(\rho - \rho_0)^2 + \beta}} [a \cos(6\phi) + 2 - a], \quad (1)$$

where $\rho_0 = 2.64$ a.u., is the radius of the molecule. The regularization parameter β is related to the screening of positive charged carbon nuclei by the core electrons; A gives the magnitude of the potential and a adjusts the height of the potential barriers between the separate Coulomb wells. In order to reduce the numerical effort of the actual calculations of HHG, Ceccherini *et al.* modified their potential model such that ionization potential exceeded the benzene experimental value by three or four times.^{24,25} We, on the other hand, choose the values of the parameters $\beta = 0.38$ a.u., $A = 0.375$ a.u., $a = 0.99$, so as to reproduce the ionization potential of real benzene ($E_{\text{ion}} = 9.25$ eV).²⁴ The effective potential [Eq. (1)] is depicted in Fig. 1.

B. Complex scaled field-free electronic states of benzene

We employ the complex-scaled field-free electronic states of benzene, $\Psi_{\theta}^{(0)}$ as a suitable basis set to describe benzene interacting with laser field (see the next Subsection). The complex-scaled field-free states are eigenstates of the field-free complex-scaled Hamiltonian,²⁸ $\hat{H}_{\theta}^{(0)}$,

$$\begin{aligned} \hat{H}_{\theta}^{(0)} &= \hat{T}_{\theta} + \hat{V}_{\theta}, \\ \hat{V}_{\theta} &= V(\rho e^{i\theta}, \phi), \\ \hat{T}_{\theta} &= -e^{-2i\theta} \frac{\hbar^2}{2m_e} \left(\frac{\partial^2}{\partial \rho^2} + \frac{1}{\rho} \frac{\partial}{\partial \rho} + \frac{1}{\rho^2} \frac{\partial^2}{\partial \phi^2} \right), \end{aligned} \quad (2)$$

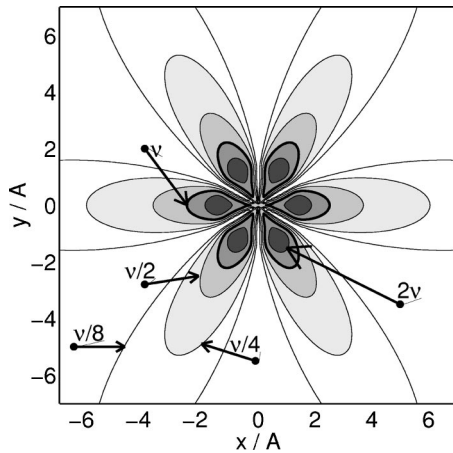


FIG. 1. One-electron effective potential used to model benzene driven by strong laser field. The potential is formed by six Coulomb wells in place of carbon atoms. The contours shown for the benzene ground state energy $v = -E_{\text{ion}} = -9.25$ eV (thick line), its multiple $2v$, and its fractions, $v/2, v/4, v/8$, demonstrate the long-range character of the model potential.

where θ is the complex scaling parameter and m_e is the electron mass. The eigenfunctions of $\hat{H}_\theta^{(0)}$ are obtained within the finite basis set approach. To this end, the C_6 symmetry-adapted “primitive” basis functions, $\{\chi_{m,k}\}$, are employed

$$\chi_{m,k} = \frac{N_{m,k}}{\sqrt{2\pi}} J_{|m|}(k\rho) e^{im\phi},$$

$$N_{m,k} = \left\{ \int_0^{\rho_{\max}} d\rho \rho [J_{|m|}(k\rho)]^2 \right\}^{-1/2}, \quad (3)$$

where m is the angular quantum number; k is the radial wave number, and ρ_{\max} is the box size. The box quantization criterion for this basis set,

$$J_{|m|}(k\rho_{\max}) = 0, \quad (4)$$

implies that different sets of discrete values of k arise for every value of $|m|$. The kinetic-energy operator is diagonal in the $\chi_{m,k}$ basis set. The elements of the kinetic-energy matrix are given by

$$\langle \chi_{m,k} | \hat{T}_\theta | \chi_{m,k} \rangle = e^{-2i\theta} \frac{\hbar^2 k^2}{2\mu}. \quad (5)$$

The potential matrix elements are given by

$$\langle \chi_{m',k'} | \hat{V}_\theta | \chi_{m,k} \rangle = \int_0^{\rho_{\max}} d\rho \rho J_{|m'|}(\rho) v(\rho e^{i\theta}, m' - m) J_{|m|}(k\rho), \quad (6)$$

where v is defined as the Fourier transform of the potential $V(\rho, \phi)$ [Eq. (1)] in the angular degree of freedom

$$v(\rho e^{i\theta}, m' - m) = \frac{1}{2\pi} \int_0^{2\pi} d\phi \exp[-i\phi(m' - m)] V(\rho e^{i\theta}, \phi). \quad (7)$$

The potential energy matrix is block-diagonal, according to the irreducible representations of the C_{6v} symmetry group.

Each one of the blocks represents coupling between the angular quantum numbers m' and m , where $\text{mod}(m',6) = \text{mod}(m,6)$.

The converged calculations of the complex scaled field-free electronic states of benzene, $\Psi_\theta^{(0)}$, require extent of the angular quantum number $-12 \leq m \leq 12$ and of the radial wave number $k \leq 12$ a.u. The need for using high values of the momenta, $\hbar k$ and $\hbar m$, is a consequence of the nearly singular character of the effective potential in the vicinity of the nuclei centers [Eq. (1)]. The box size, ρ_{\max} , necessary for the convergence of the driven electron wave functions (see the next Subsection), is $\rho_{\max} \approx 16$ Å. This box size allows us to resolve 17 bound states of the model potential, which are mostly the Rydberg states. The field free complex scaled electronic states of benzene are constructed typically from 3000 to 3500 primitive basis functions.

C. Quasi-energy Floquet resonance states by the (t, t') -method

The interaction of the laser field with the benzene molecule is described within the dipole approximation. The complex-scaled Hamiltonian in the reduced momentum gauge is given by

$$\hat{H}_\theta = \hat{H}_\theta^{(0)} + \frac{i\hbar}{2m_e c} e \vec{A} \cdot \hat{\nabla}, \quad (8)$$

where c is the speed of light and e is the electronic charge. The vector potential of the electric field, \vec{A} , is given by

$$A_x = c E_0 \omega^{-1} \sin \omega t \cos \alpha,$$

$$A_y = -c E_0 \omega^{-1} \cos \omega t \sin \alpha, \quad (9)$$

where ω is the laser frequency ($\omega = 0.057$ a.u., corresponding to wave-length $\lambda = 800$ nm); E_0 is the laser field amplitude, $0.005 < E_0 < 0.06$ a.u., which implies that the laser intensity, I_0 , is varied within the interval, $1 < I_0 < 125$ TW cm $^{-2}$. The ellipticity of the electric field, ϵ , is determined by the parameter α , $\epsilon = \tan \alpha$. In our calculations, the ellipticity varies within the interval of, $0.94 \leq \epsilon \leq 1$.

The Hamiltonian \hat{H}_θ [Eq. (8)] with the vector potential \vec{A} [Eq. (9)] can be represented as

$$\hat{H}_\theta = \hat{H}_\theta^{(0)} + \hat{\mu}_{\theta+} e^{i\omega t} + \hat{\mu}_{\theta-} e^{-i\omega t}, \quad (10)$$

where $\hat{H}_\theta^{(0)}$ is the field free complex scaled Hamiltonian [Eq. (2)], and $\hat{\mu}_{\theta\pm}$ are the transition dipole moment operators given by

$$\hat{\mu}_{\theta\pm} = \frac{E_0 e}{2m_e \omega} (\pm i \hat{p}_{\theta x} \cos \alpha + \hat{p}_{\theta y} \sin \alpha). \quad (11)$$

Here \hat{p}_x , \hat{p}_y are the complex-scaled momentum operators, $\hat{p}_{\theta x} = -i\hbar e^{-i\theta} \partial / \partial x$, $\hat{p}_{\theta y} = -i\hbar e^{-i\theta} \partial / \partial y$. The meta-stable (resonance) quasi-energy states of driven benzene, Φ_θ , are eigenfunctions of the complex scaled Floquet operator which is defined as

$$\hat{F}_\theta(\rho, \phi, t) = -i\hbar \frac{\partial}{\partial t} + \hat{H}_\theta. \quad (12)$$

The Floquet operator is represented in the basis set of the field free complex scaled electronic states of benzene, $\Psi_\theta^{(0)}$, and $2N_t + 1$ time-dependent Fourier basis functions (“frequency channels”), $\exp(i\omega nt)$, $n = 0, \pm 1, \dots, \pm N_t$. The matrix representation of the Floquet operator, \mathbf{F}_θ , is a super-matrix which consists of elements, $\{\mathbf{F}_\theta\}_{n',n}$, coupling between frequency channels

$$\{\mathbf{F}_\theta\}_{n',n} = \delta_{n',n}(n\hbar\omega + \mathbf{E}_\theta^{(0)}) + \delta_{n',n+1}\mathbf{M}_{\theta+} + \delta_{n',n-1}\mathbf{M}_{\theta-},$$

$$\{n, n'\} = -N_t \dots N_t, \quad (13)$$

where $\mathbf{E}_\theta^{(0)}$ is the diagonal matrix of the complex eigen-energies of the field-free Hamiltonian, $\hat{H}_\theta^{(0)}$. The transition dipole matrices, $\mathbf{M}_{\theta\pm}$, represent the operators $\hat{\mu}_{\theta\pm}$ [Eq. (11)] in the basis set of the eigenstates of the field free Hamiltonian, $\Psi_\theta^{(0)}$. The numerical evaluation of the transition dipole matrix elements is described in detail in the Appendix. The eigenvalues and eigenfunctions of the Floquet operator are calculated using the time-evolution approach. The diagonalization of the time-evolution matrix, \mathbf{u}_θ , for the time period of one optical cycle, provides the eigenvalues, Λ_θ , and eigen-vectors, \mathbf{c}_θ , where the right eigenvectors of the non-Hermitian nonsymmetric matrix \mathbf{u}_θ are used. The matrix \mathbf{u}_θ is calculated by the means of the (t, t') -method,^{29,34}

$$\mathbf{u}_\theta = \prod_{m=1}^{M_t} \sum_{n=-N_t}^{N_t} \exp(-i\omega nm\tau) \left\{ \exp\left(-\frac{i}{\hbar}\mathbf{F}_\theta\tau\right) \right\}_{n,0},$$

$$\tau = 2\pi/\omega M_t, \quad (14)$$

where M_t is the number of the propagation time steps and τ is the time step. The curly brackets denote the sub-matrices of the super-matrix for the specified frequency channels. The eigenvalues of the Floquet operator are obtained from the eigenvalues of the time-evolution matrix for one optical cycle, Λ_θ . The complex eigenvalues of the Floquet operator, $E_\theta - (i/2)\Gamma_\theta$, are given by

$$E_\theta = -\frac{\hbar\omega}{2\pi} \Im \log \Lambda_\theta + \hbar\omega n, \quad n = 0, \pm 1, \dots,$$

$$\Gamma_\theta = -\frac{\hbar\omega}{\pi} \Re \log \Lambda_\theta. \quad (15)$$

The convergence criterion for the resonance quasi-energy, E , and width, Γ , with respect to the scaling parameter θ , is given by the stationarity condition²⁸

$$\left. \frac{\partial E_\theta}{\partial \theta} \right|_{\theta_0} = \left. \frac{\partial \Gamma_\theta}{\partial \theta} \right|_{\theta_0} = 0, \quad E = E_\theta|_{\theta_0}, \quad \Gamma = \Gamma_\theta|_{\theta_0}. \quad (16)$$

Floquet resonance states, $\Phi_\theta = \Phi_\theta(\rho, \phi, t)$, are time-periodic with the period $T = 2\pi/\omega$. The eigenvectors, \mathbf{c}_θ , of the time-evolution matrix \mathbf{u}_θ represent the Floquet states at $t = nT$, $n = 0, \pm 1, \dots$, in the basis set of $\Psi_\theta^{(0)}$. The vectors \mathbf{c}_θ are evolved in time along one optical cycle using the recursive relation

$$\mathbf{c}_\theta(t) = \mathbf{u}_{\theta\tau}(t \leftarrow t - \tau) \mathbf{c}_\theta(t - \tau), \quad \mathbf{c}_\theta(t=0) = \mathbf{c}_\theta, \quad (17)$$

where the one step propagation matrix $\mathbf{u}_{\theta\tau}$ is given by the transform to the frequency representation

$$\mathbf{u}_{\theta\tau}(t \leftarrow t - \tau) = \sum_{n=-N_t}^{N_t} \exp(-i\omega nt) \times \left\{ \exp\left(-\frac{i}{\hbar}\mathbf{F}_\theta\tau\right) \right\}_{n,0}. \quad (18)$$

The eigenvectors \mathbf{C}_θ of the Floquet matrix \mathbf{F}_θ [Eq. (13)], are given by

$$\{\mathbf{C}_\theta\}_{n,0} = \frac{\omega}{2\pi} \int_0^{2\pi/\omega} \mathbf{c}_\theta(t) \exp(in\omega t) dt, \quad (19)$$

where the curly brackets denote the sub-matrices of the super-matrix.

The converged calculations of quasi-energy resonances are performed using the basis set of 650 field-free states of benzene, $\Psi_\theta^{(0)}$, which implies that the basis for the electron spans the energy interval up to 4 a.u. above the ionization threshold. The converged number of frequency channels is varied within the interval, $17 \leq N_t \leq 23$, according to the laser intensity I_0 . The converged number of time steps is $M_t = 1000$. The optimal scaling parameter, θ_0 , varies within the interval $0.02 \leq \theta_0 \leq 0.2$ rad.

D. Calculation of high-order harmonic generation spectrum

The benzene molecule interacting with the strong laser field of the frequency ω , generates high-order harmonic frequencies, $n\omega$, where n is an integer. The intensities of the generated high-order harmonics, $I(n\omega)$, are calculated as a sum of the intensities of radiation polarized along x and y axes

$$I(n\omega) = I_x(n\omega) + I_y(n\omega). \quad (20)$$

In the following we describe only the calculation of the x -contribution to the intensity I_x , since the calculation of the other contribution, I_y , is analogous. $I_x(n\omega)$ is obtained within the dipole approximation, from the induced dipole moment, $\mu_x(t)$:

$$I_x(n\omega) \propto \left| \int_0^{2\pi/\omega} \frac{d^2 \mu_x(t)}{dt^2} \exp(-in\omega t) dt \right|^2$$

$$\propto n^4 |\eta_x(n\omega)|^2, \quad (21)$$

where $\eta_x(n\omega)$ is the Fourier transform of the induced dipole moment

$$\eta_x(n\omega) = \frac{\omega}{2\pi} \int_0^{2\pi/\omega} \mu_x(t) \exp(-in\omega t) dt. \quad (22)$$

The molecule which occupies the resonance Φ_{θ_j} possesses the complex-scaled (θ -dependent) induced dipole moment $\mu_{\theta_x}(t)$

$$\mu_{\theta_x}(t) = \int \int \Phi_{\theta_j}^{(l)}(\rho, \phi, t) \hat{p}_{\theta_x} \Phi_{\theta_j}^{(r)}(\rho, \phi, t) \rho d\rho d\phi, \quad (23)$$

where the upper indexes (l) and (r) specify the left and right eigenfunction Φ_{θ_j} of the complex scaled (non-Hermitian) Floquet operator [Eq. (12)] and \hat{p}_{θ_x} is the complex scaled

momentum operator. The matrix representation of the Floquet state $\Phi_{\theta j}$ in the basis of the field free complex scaled electronic states of benzene, $\Psi_{\theta}^{(0)}$, and time dependent Fourier basis functions, $\exp(i\omega n t)$, is given by the j th column of the sub-matrices $\{\mathbf{C}_{\theta}\}_{n,0}$ in the super-matrix \mathbf{C}_{θ} . We specify the column index of the sub-matrix by putting the superscript, $\{\mathbf{C}_{\theta}\}_{n,0}^j$. The frequency representation of the complex-scaled induced dipole moment, $\eta_{\theta x}(n\omega)$, [Eq. (22)] is calculated using the equation

$$\eta_{\theta x}(n\omega) = \sum_{n'=-N_t}^{N_t} (\{\mathbf{C}_{\theta}\}_{n'-n,0}^j)^t \mathbf{P}_{\theta x} \{\mathbf{C}_{\theta}\}_{n',0}^j, \quad (24)$$

where $\mathbf{P}_{\theta x}$ represents the operator $\hat{p}_{\theta x}$ in the basis set of $\{\Psi_{\theta}^{(0)}\}$. The evaluation of the matrix $\mathbf{P}_{\theta x}$ with the use of the primitive basis set is described in the Appendix. The θ -converged values of $\eta_x(n\omega)$ are obtained as the ones satisfying the stationarity condition for every value of n

$$\left. \frac{\partial \Re \eta_{\theta x}(n\omega)}{\partial \theta} \right|_{\theta_0(n)} = \left. \frac{\partial \Im \eta_{\theta x}(n\omega)}{\partial \theta} \right|_{\theta_0(n)} = 0,$$

$$\eta_x(n\omega) = \eta_{\theta x}(n\omega) \Big|_{\theta_0(n)}. \quad (25)$$

III. RESONANCE QUASI-ENERGY STATES OF BENZENE IN STRONG CIRCULAR POLARIZED LASER FIELD

A. Ionization rate

The Floquet calculations of the type presented in this work are especially useful when the strong-field dynamics is dominated by a single resonance quasi-energy state. Assuming that the laser field has a form of a pulse, e.g., a Gaussian one, one can formulate the necessary conditions for the adiabatic transfer of the population from an electronic ground state to the corresponding resonance state (see Refs. 30 and 31). In particular, it is required that the pulse includes enough optical cycles of the driving field for its envelope to change slowly within one optical cycle. Typically, a pulse covering several tens of field oscillations (≥ 50 fs for $\lambda = 800$ nm) can be thought of as long enough. In addition, the lifetime of the ground-state resonance must remain significantly larger than the lifetimes of the other resonances.

The quasi-energies and widths of the Floquet resonances are calculated using complex scaling approach and the (t, t') -method, as described in Sec. II C. The resonance widths, Γ_j , provide the ionization rate of driven benzene. Γ_j are calculated for the range of the laser intensities $1 < I_0 < 90$ TW cm $^{-2}$, see Fig. 2(a). The corresponding resonance lifetime is $\tau = 1/\Gamma$, see the right axis in Fig. 2(a). The width of the ground-state resonance is negligible, $\Gamma_0 \approx 0$, for the range of small laser intensities, $1 < I_0 < 39$ TW cm $^{-2}$. The corresponding resonance life-time exceeds 100 fs. On the other hand, for a large laser intensity, $I_0 = 90$ TW cm $^{-2}$, Γ_0 reaches the value of 0.07ω , where the corresponding resonance life-time is as short as $\tau = 6$ fs. The ground-state reso-

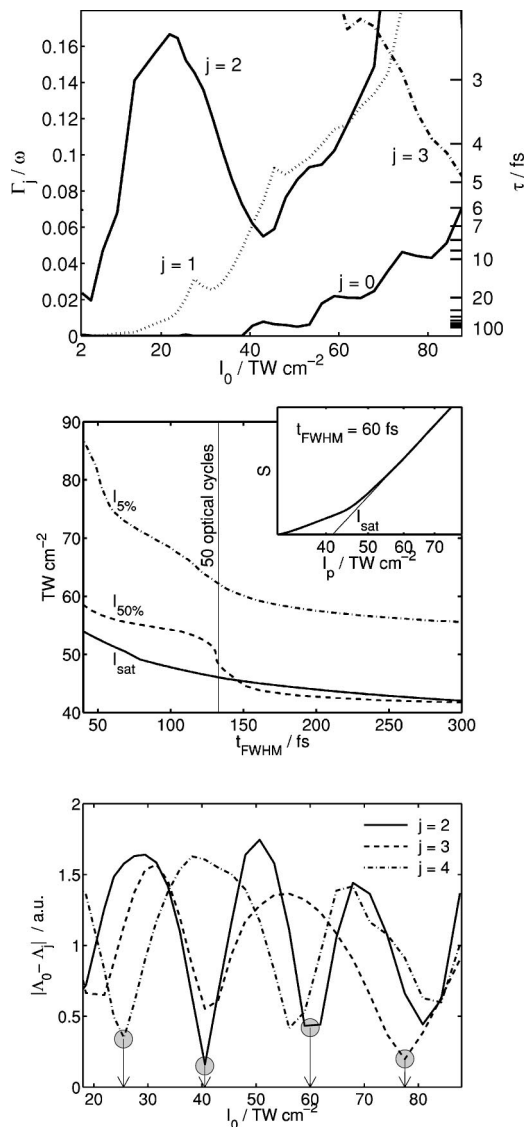


FIG. 2. (a) Resonance widths Γ_j for the ground state resonance ($j=0$), and for the resonances with relatively small widths ($j=1,2,3$). The corresponding life-time $\tau=1/\Gamma$ is given by the right axis. (b) The saturation intensity I_{sat} for the parallel Gaussian beam ($\lambda=800$ nm) is given by the solid line. The dashed line shows the intensity $I_{50\%}$, where 50% of molecules are ionized when the pulse reaches its maximum. The dot-dashed line shows the intensity $I_{5\%}$, where 5% of molecules are ionized when the pulse reaches its maximum. The optimum adiabatic pulse is delimited by I_{sat} and $I_{5\%}$. Small panel provides an example of the ion signal dependence on the peak intensity of the Gaussian beam for the pulse length 60 fs. The definition of I_{sat} is illustrated. (c) The distance of resonances $j=2, 3, 4$ from the longest-lived resonance within the unit circle, $|\Lambda_0 - \Lambda_j|$, shows a number of avoided crossings between the resonances, concentrated in regions where the laser intensity $I_0 \approx 25, 38, 58, 75$ TW cm $^{-2}$.

nance remains the longest-lived one for the studied interval of intensities $1 < I_0 < 90$ TW cm $^{-2}$, thus the second condition for the pulse adiabaticity is satisfied.

Γ_0 can be converted to saturation intensity for a parallel Gaussian beam, I_{sat} , which is defined by the linear onset of ion signal in logarithmic scale.³⁵ The ion signal, S , produced by a parallel Gaussian beam of peak intensity I_p is given by³⁵

$$S(I_p) \propto \int_0^{I_p} \frac{1 - \aleph(I_m)}{I_m} dI_m, \quad (26)$$

where \aleph is the survival probability of the neutral charged system after the pulse completion. The integration is performed over the pulse intensity at the maximum, I_m , all the way from sides to the center of the laser beam. Using the adiabatic pulse approximation, \aleph is given by

$$\aleph(I_m) = \exp\left(-\frac{1}{\hbar} \int_{-\infty}^{\infty} \Gamma[I_0(t)] dt\right). \quad (27)$$

$I_0(t)$ is the intensity of the Gaussian laser pulse given by

$$I_0(t) = I_m \exp(-\ln 2 t^2 / t_{\text{FWHM}}^2), \quad (28)$$

where t_{FWHM} is the pulse duration (full width at half maximum) (see, e.g., Ref. 36). The values of I_{sat} are presented in Fig. 2(b) for the range of pulse durations $40 \text{ fs} < t_{\text{FWHM}} < 300 \text{ fs}$. The sub-panel of Fig. 2(b) demonstrates a typical ion signal dependence on the peak beam intensity I_p , where the pulse length is chosen to be $t_{\text{FWHM}} = 60 \text{ fs}$. It illustrates the definition of I_{sat} . The relative portion of neutral molecules when the laser pulse reaches its maximum intensity is given by

$$P(I_m) = \exp\left(-\frac{1}{\hbar} \int_{-\infty}^0 \Gamma[I_0(t)] dt\right). \quad (29)$$

The contours for $P(I_{50\%}) = 0.5$, and $P(I_{5\%}) = 0.05$, are plotted on Fig. 2(b) side by side with I_{sat} . Clearly, the saturation intensity for a parallel Gaussian beam implies approximately that 50% of molecules are ionized when the pulse reaches its maximum. The optimum choice for an adiabatic pulse is delimited by the saturation intensity. In principle, the HHG should be observable even at higher intensity, e.g., at $I_{5\%}$, but the efficiency is supposed to be trimmed down by the ionization.

B. Field-dependent avoided crossings

The resonance width of the ground-state resonance, Γ_0 , shows a step-wise structure [Fig. 2(a)]. The sudden enhancements of the ionization rate for the specific laser intensities correspond to the increased interaction between the longest-lived resonance and the short-lived resonances. The interaction between resonances takes place when their quasi-energies approach one another in the complex energy plane.³⁰ Since the Floquet energies form a periodic pattern [Eq. (15)], it is convenient to search avoided crossings within the unit circle, where Λ_j represents the resonance quasi-energy E_j and width Γ_j

$$\Lambda_j = \exp\left(-i \frac{2\pi}{\hbar \omega} E_j\right) \exp\left(-\frac{\pi}{\hbar \omega} \Gamma_j\right). \quad (30)$$

In Fig. 2(c) we plot the distance between the resonances within the unit circle, $|\Lambda_0 - \Lambda_j|$, as a function of the laser intensity. The ground-state resonance is approached by several other resonances for the laser intensities $I_0 = 25 \pm 5$, 38 ± 5 , 58 ± 5 , $75 \pm 5 \text{ TW cm}^{-2}$. These are exactly the regions of the increased ionization rate. The association of nonlinear effects with field-dependent multiple avoided crossings has

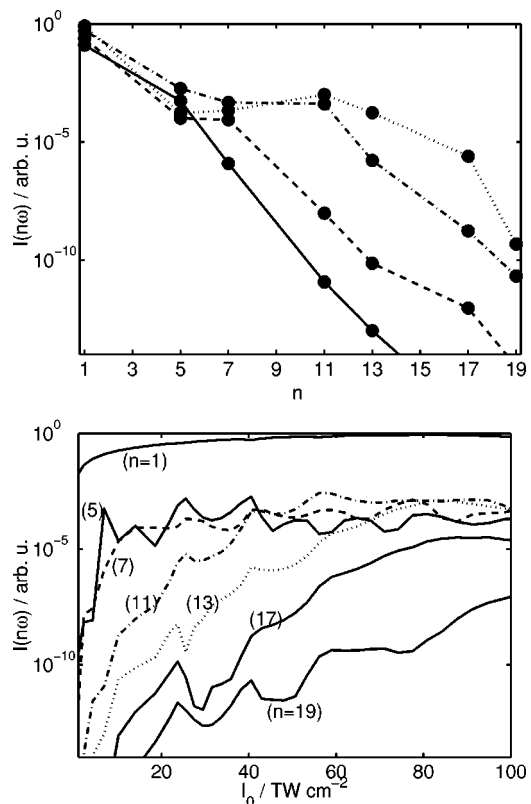


FIG. 3. (a) Selective high-order harmonic generation spectra of aligned benzene in circular polarized laser field for different laser intensities, $I_0 = 7 \text{ TW cm}^{-2}$ (solid line), $I_0 = 14 \text{ TW cm}^{-2}$ (dashed line), $I_0 = 40.5 \text{ TW cm}^{-2}$ (dot-dashed line), and $I_0 = 68 \text{ TW cm}^{-2}$ (dotted line). (b) The intensities of the symmetry allowed high-order harmonics $\omega, 5\omega, 7\omega, \dots, 19\omega$, as functions of the intensity of the laser field.

been recognized previously for a one-dimensional model of the Xe atom.³⁰ A strong effect of multiple avoided crossings leading to a creation of HHG plateau has been reported for the case of the He atom.³¹ The effect of avoided crossing on the Floquet wave functions has been studied in detail for a one-dimensional sinusoidally driven square well.³² A periodic enhancement of HHG, similar to the one which is to be discussed in the next Section of our study, has been observed in atoms and assigned to the interaction of the ground-state resonance with atomic Rydberg resonances.³³

IV. SELECTIVE HIGH-ORDER HARMONIC GENERATION IN BENZENE BY CIRCULAR POLARIZED LASER FIELD

A. High-order harmonic generation spectrum

The high-order harmonic generation spectrum of the benzene molecule interacting with the circular polarized field is presented in Fig. 3(a). Four spectra are plotted, each obtained for a different laser intensity, I_0 . The high-order harmonic frequencies $n\omega$, $n \in \{1, 5, 7, 11, 13, 17, 19, \dots\}$, appear in the HHG spectrum, while the other frequencies are forbidden according to the DS-based selection rules for the C_6 symmetry molecules in the circular polarized light.¹⁸ The selected set of HHG spectra for the different laser intensities, $I_0 = 7, 14, 40.5, 68 \text{ TW cm}^{-2}$, demonstrates the increase of the length of the HHG plateau. The more detailed Fig. 3(b)

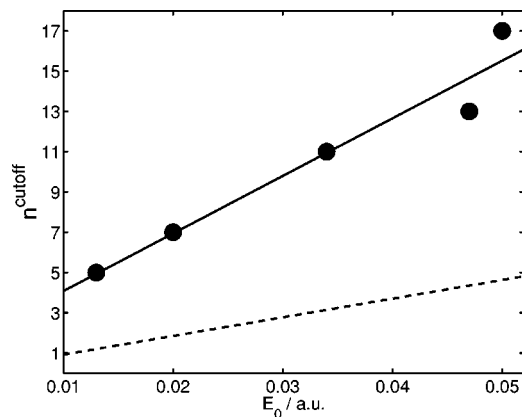


FIG. 4. The cut-off position dependence on the amplitude of the circular polarized laser field, E_0 . The symbols show the cut-off position at the allowed 5th, 7th, ..., 17th high-order harmonics. The solid line is a linear fit for the dependence of the cut-off position on the laser amplitude. The estimate of the cut-off position (dashed line) using the simple approximation for the typical transition dipole moment, $\mu_{tr} = e\rho_0$ [see Eq. (31)].

shows the growth of high harmonic intensities I_n , $n \in \{1, 5, 7, 11, 13, 17, 19, \dots\}$, as functions of the laser intensity, I_0 . The intensities I_n of the separate high-order harmonics grow roughly exponentially with the increasing laser intensity I_0 , until they join the plateau. At the intensities, where the high-order harmonics join the plateau, the length of the plateau is well defined. The plateau length, n_{cutoff} , is plotted with respect to the laser amplitude, E_0 , in Fig. 4, giving an evidence that the growth of the plateau is linear with the laser strength parameter. This is in agreement with the predictions based on a simplified bound state model,²⁰ which predicts the following dependence of the cutoff on the laser amplitude:

$$n_{\text{cutoff}} = \frac{2E_0\mu_{tr}}{\hbar\omega}. \quad (31)$$

In Ref. 20 it has been assumed that the typical transition dipole moment, μ_{tr} , is given by $e\rho_0$, where ρ_0 is the molecular radius [Eq. (1)]. The theoretical prediction for the plateau length using this assumption is shown in Fig. 4 by the dashed line. It turns out that the length of the plateau is underestimated by the simple theory approximately by a factor of four. The reason is that the transition dipole moments to diffuse benzene states, where $\mu_{tr} > e\rho_0$, play a non-negligible role in the HHG process.

The intensities of high-order harmonics, $I(n\omega)$, do not depend monotonically on the laser intensity, I_0 , but embody a spiked structure [see Fig. 3(b)]. Figures 5(a) and 5(b) show the intensities of the plateau harmonics on the linear scale [the 5th and 7th harmonics are plotted in Fig. 5(a), the 11th and 13th harmonics are plotted in Fig. 5(b)]. The enhancements of the HHG by one order of magnitude are observed for the 5th harmonic at laser intensities $I_0 = 22, 39 \text{ TW cm}^{-2}$, for the 7th harmonic at laser intensities $I_0 = 75 \text{ TW cm}^{-2}$, for 11th harmonic at $I_0 = 57 \text{ TW cm}^{-2}$, and the 13th harmonic is enhanced at $I_0 = 82 \text{ TW cm}^{-2}$. The enhancement of the high-order harmonic generation is directly correlated with the increased interaction of the longest-lived resonance with other resonances. The avoided cross-

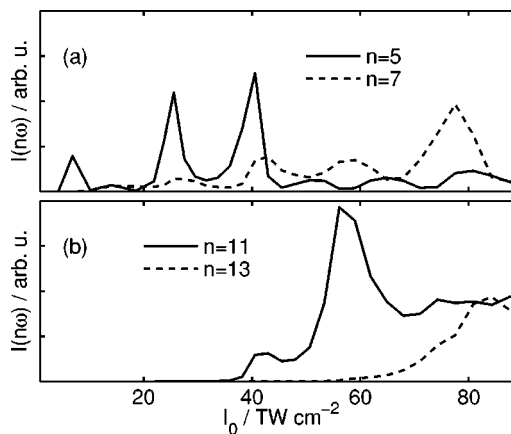


FIG. 5. The intensities $I(n\omega)$ of the plateau high-order harmonics are plotted in the linear scale with respect to the incident laser intensity. (a) The 5th harmonic (solid line) manifests the factor of 2 to 3 enhancements for the laser intensities $I_0 = 25 \text{ TW cm}^{-2}$ and $I_0 = 40 \text{ TW cm}^{-2}$. The 7th harmonic (dashed line) manifests the factor of two enhancement for $I_0 = 67 \text{ TW cm}^{-2}$. (b) The 11th harmonic (solid line) joins the plateau at $I_0 = 30 \text{ TW cm}^{-2}$, and manifests factor of four enhancement for $I_0 = 58 \text{ TW cm}^{-2}$. The 13th harmonic (dashed line) joins the plateau at $I_0 = 55 \text{ TW cm}^{-2}$, and manifests the factor of two enhancement for $I_0 = 83 \text{ TW cm}^{-2}$.

ings of the ground state resonance with other resonances in complex energy plane occur for the very same incident laser intensities as the enhancements of the high-order harmonic intensities (see Sec. III).

B. The mechanism of the selective HHG

The detailed data on the intensity dependences of the emitted high-order harmonics presented in Sec. IV A allow us to investigate the mechanism of the selective HHG. The observed linear growth of the benzene HHG plateau with the laser field amplitude represents one evidence suggesting that the transitions between the bound states of the molecule are mainly responsible for the generation of the high-order harmonics. This proposition has been substantiated in Ref. 20 by the fact that the bound-continuum contribution to the molecular HHG at circular polarization is quite small due to the lack of the “rescattering” trajectories of the ionized electrons returning to the vicinity of the molecule with high kinetic energy.

Further evidence for the dominance of the bound-bound transitions in the molecular HHG process comes from the comparison of the numerically converged intensity dependences of the high-order harmonics with the results of the truncated twelve-state model calculations. In Fig. 6 we present the intensity dependences of the high-order harmonics resulting both from the full calculation including the continuum and from the truncated calculation in which only the transitions between twelve low-energy bound states of the model potential [Eq. (1)] are allowed. One can observe a reasonable qualitative agreement between the two results. The general similarity between the correct and the bound model intensity dependences clearly shows that the bound-bound transitions play the dominant role in the emission of

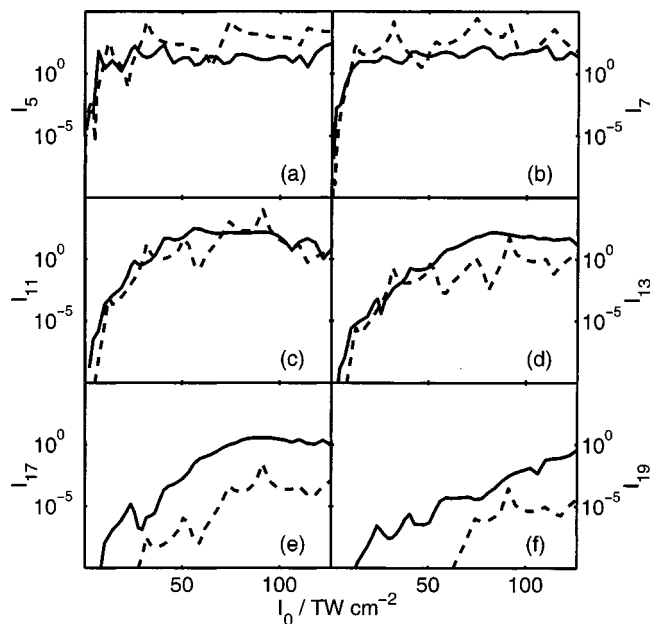


FIG. 6. High-order harmonics intensities as functions of the laser intensity: (a) 5th harmonic, (b) 7th harmonic, (c) 11th harmonic, (d) 13th harmonic, (e) 17th harmonic, and (f) 19th harmonic. The solid lines represent the numerically exact result, while the dashed lines are obtained by the approximation using 12 bound field-free states of benzene for representing Floquet states. The qualitative agreement between the two results explains the mechanism of molecular HHG in circular polarized field.

the high-order harmonics by benzene interacting with circular polarized field.

It is easy to notice a few characteristic differences between the results of the full and the bound model calculations (see Fig. 6). First of all, the bound model does not reproduce correctly the pattern of oscillations in the high-order harmonic intensities. This would be quite natural to expect since the enhancements of the particular harmonics correspond to the avoided crossings of various resonance states in complex quasi-energy plane. The bound model is unable to reproduce correctly the ac Stark shifts defining the intensity dependence of the real parts of the quasi-energies. Moreover, it cannot in principle predict the life-times of the relevant resonance states. Thus, the avoided crossing events, and with them the enhancements of the high-order harmonics, cannot be reliably predicted by a bound model. Despite the noncompatible oscillation patterns in the numerically converged and the bound model results, one can observe that the exact average intensities of the 5th and the 7th harmonics in the plateau region ($I_0 \geq 25 \text{ TW cm}^{-2}$) are at least one order of magnitude lower than their twelve-state counterparts. This occurs due to the depletion of the bound state populations by ionization. Indeed, the ionized electrons do not contribute significantly to the HHG process,²⁰ thus the bound model which does not take the ionization into account, tends to overestimate the HHG efficiency. On the other hand, the exact intensities of the higher-order 17th and 19th harmonics, barely reaching the plateau at the considered field intensities, are higher than those predicted by the bound model. This shows that the high-energy Rydberg states and the continuum states are of some importance for the generation of

the low-intensity harmonics in the cutoff region of the HHG spectrum. Apparently, the 11th and the 13th harmonics which are well reproduced on average by the bound model, constitute the intermediate case where both the depletion of the low-energy states and the population of the high-energy states affect the HHG process.

Our calculations reveal that the mechanism of the molecular HHG in circular polarized field is dramatically different from the well-known rescattering mechanism^{5,6} characteristic of atomic HHG in linear polarized field. It is clear, on the other hand, that as the field ellipticity decreases from one to zero, the rescattering of the ionized electron on the molecular ion becomes more and more probable and as a consequence, the bound–continuum transitions start to play a major role in the HHG process. Eventually, at zero ellipticity the familiar atomic plateau extending up to about $E_{\text{ion}} + 3.2U_p$ is expected to be formed. For the field frequency and the moderate intensities considered in this work, the length of this rescattering plateau is of the same order of magnitude as the length of the bound–bound plateau appearing at the corresponding field parameters at circular polarization. One can speculate thus, that both bound–bound and bound–continuum transitions are important for the benzene HHG at linear polarization. This scenario, if indeed true, would be similar to the situation in alkali atoms, where the non-negligible contribution of the first excited state to the atomic HHG has been identified.³⁸ The actual verification of this conjecture as well as the numerical determination of the ellipticity dependences of the high-order harmonics in the entire ellipticity range is beyond the scope of the present work. However, two more considerations of the qualitative nature can be brought here. First, the DS-based selection rules holding at circular polarization break down at nonunity ellipticity. Their stability with respect to small ellipticity deviations is considered in the next section. Second, the efficiency of the rescattering process is determined not only by the field polarization, but also by the molecular orientation and the nodal structure of the ionized molecular orbital.³⁹ Thus, the relative importance of the bound–bound and bound–continuum transitions for the HHG of oriented benzene even at the linear polarization represents an interesting problem for future studies.

V. STABILITY OF THE SELECTION RULES WITH RESPECT TO THE DEVIATIONS OF ELLIPTICITY AND MOLECULAR ALIGNMENT

The selection rules for the harmonic generation in benzene, hold under the conditions of the ideal benzene alignment and the exact circular polarization of the laser. In this Section we discuss the stability of the selection rules for benzene provided that the laser polarization and the molecular alignment are not ideal. The deviation from the circular polarization of the field is given by the nonunity ellipticity ϵ [Eq. (9) and text below]. The polarization axis bisects the carbon atoms in our calculation. The emission amplitudes depend on the ellipticity ϵ , as illustrated in Fig. 7(b) for the incident laser intensity $I_0 = 56 \text{ TW cm}^{-2}$. The high-order harmonics which are allowed for the elliptic polarization subdivide into two classes: the “circular allowed” class, n

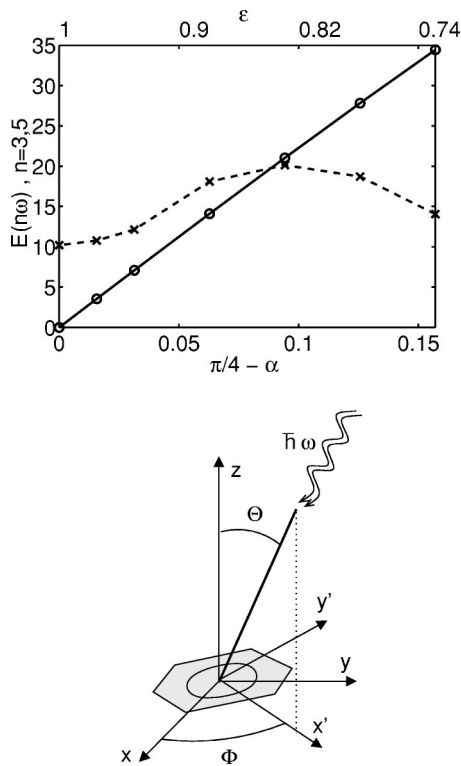


FIG. 7. (a) Amplitudes of high-order harmonics for a small deviation of the field ellipticity from unity. The intensity of the 3rd harmonics, representing the class of circularly forbidden harmonics $(6l \pm 3)\omega$, grows linearly with $(\pi/4 - \alpha)$ (solid line). The intensity of the 5th harmonics, representing the class of circularly allowed harmonics $(6l \pm 1)\omega$, acquires zero first derivative at $\epsilon = 1$. (b) The deviation from alignment as given in molecular frame x, y, z by angles Φ, Θ and is transformed into the deviation from ellipticity (see Sec. V).

$= 6l \pm 1$, and the “circular forbidden” class, $n = 6l \pm 3$, ($l = 1, 2, \dots$). The symmetry analysis of the first-order perturbation correction to the Floquet state provides the functional dependence of the HHG amplitudes on the ellipticity parameter α for the small deviation from the circular polarization.¹⁸ It can be shown that the emission amplitudes of circular forbidden harmonics, $E[(6l \pm 3)\omega]$, increase linearly with the ellipticity parameter α , while the amplitudes of the circular allowed harmonics, $E[(6l \pm 1)\omega]$, are constant with α in the linear approximation. Figure 7(b) demonstrates this rule for benzene. The amplitude of the symmetry forbidden third-order harmonics is linear for $0.8 \leq \epsilon \leq 1$. The amplitude of the fifth-order harmonics remains constant to a good approximation for $0.95 \leq \epsilon \leq 1$.

The selection rules are observed in the HHG spectrum whenever the circular forbidden harmonics are considerably less pronounced than the circular allowed harmonics. Suppose factor f of depletion of circular forbidden harmonics is needed in order to demonstrate selection rules. Then, the maximum permissible ellipticities, $\epsilon_{5/3}, \epsilon_{7/9}$ can be defined by

$$\left. \frac{I(5\omega)}{I(3\omega)} \right|_{\epsilon_{5/3}} = f, \quad \left. \frac{I(7\omega)}{I(9\omega)} \right|_{\epsilon_{7/9}} = f. \quad (32)$$

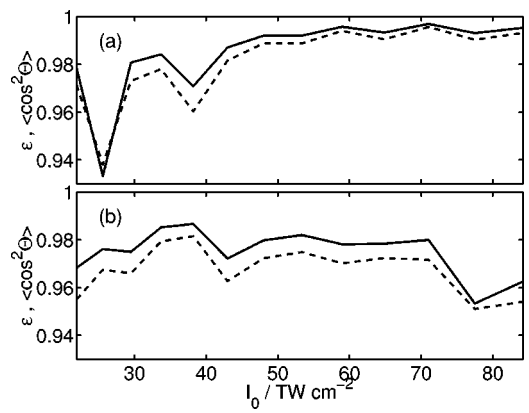


FIG. 8. The ellipticity (ϵ , solid lines) and the degree of alignment ($\langle \cos^2 \Theta \rangle$, dashed lines) which are necessary to achieve in order to observe the factor of fifty suppression of (a) the 3rd harmonics with respect to 5th harmonics, (b) the 9th harmonics with respect to 7th harmonics, due to selection rules for aligned benzene in circular polarized field.

The specific choice for the value of the factor f depends on the overall character of the HHG spectrum. The plateau harmonics usually oscillate in their intensities by a factor of four due to avoided crossings of resonances which are unrelated to the selection rules. Therefore, the selection rules are observed whenever the suppression of circular forbidden harmonics reaches the factor $f \gg 4$. Here, we adopt the value of $f = 50$. The maximum permissible ellipticities are found using the approximative perturbative dependence of intensities on the ellipticity parameter, α

$$I[(6l \pm 1); \alpha] = I[(6l \pm 1); \alpha = 0] = \text{const.}, \quad (33)$$

$$I[(6l \pm 3); \alpha] = \frac{1}{\Delta^2} \left(\frac{\pi}{4} - \alpha \right)^2 I[(6l \pm 3); \alpha = \left(\frac{\pi}{4} - \Delta \right)],$$

where the small deviation from the circular polarization $\Delta = 0.01\pi$ is used, which corresponds to the ellipticity $\epsilon = 0.94$. The values of the maximum permissible ellipticities, $\epsilon_{5/3}, \epsilon_{7/9}$, for different laser intensities, $22 \leq I_0 \leq 84 \text{ TW cm}^{-2}$ are presented in Figs. 8(a) and 8(b). The selection rules are best observed for the incident laser intensities $I_0 < 30 \text{ TW cm}^{-2}$, where the required accuracy of the circular polarization is less than 5%.

The deviation from the ideal alignment can be approximately transformed to the deviation from the circular polarization. The molecular alignment with respect to the propagation axis of the field is given by the angles Θ, Φ , see Fig. 7(a). The imperfectly aligned molecule is driven by the circular polarized electric field, described by the following vector potential:

$$\begin{aligned} A_{x'} &= \sqrt{2}cE_0\omega^{-1} \sin \omega t \cos \Theta, \\ A_{y'} &= -\sqrt{2}cE_0\omega^{-1} \cos \omega t, \\ A_z &= -\sqrt{2}cE_0\omega^{-1} \cos \omega t \sin \Theta. \end{aligned} \quad (34)$$

The effect of the A_z component of the vector potential cannot be described using the two-dimensional model. However, A_z can be neglected for a small deviation from the ideal alignment, $\Theta \rightarrow 0$, which is considered here. The in-plane compo-

nents create the elliptic polarized electric field, characterized by the Θ dependent effective intensity, E_0^{eff} , and parameter of ellipticity, α

$$\begin{aligned} A_{x'} &= \sqrt{2}cE_0^{\text{eff}}\omega^{-1}\sin\omega t\cos\alpha, \\ A_{y'} &= -\sqrt{2}cE_0^{\text{eff}}\omega^{-1}\cos\omega t\sin\alpha, \\ \alpha &= \arctan\frac{1}{\cos\Theta}, \\ E_0^{\text{eff}} &= E_0\sqrt{\frac{1+\cos^2\Theta}{2}}. \end{aligned} \quad (35)$$

Using the Eq. (35) one can calculate the HHG by an imperfectly aligned molecule, using the two-dimensional model. The molecules aligned by low intensity laser field obey the statistical distribution given by¹⁴

$$\zeta_\sigma(\Theta, \Phi) = \exp\left(-\frac{\sin^2\Theta}{2\sigma^2}\right), \quad (36)$$

where the width of the distribution, σ , is directly related to the degree of alignment, $\kappa = \langle \cos^2\Theta \rangle$, given by

$$\kappa(\sigma) = \int_0^{2\pi} \int_0^\pi \zeta_\sigma(\Theta, \Phi) \cos^2\Theta \sin\Theta d\Theta d\Phi. \quad (37)$$

The average harmonics emission intensity, $\bar{I}(n\omega)$, of a sample which is characterized by the distribution ζ_σ , is given by

$$\begin{aligned} \bar{I}[n\omega; \sigma(\kappa)] &= \int_0^{2\pi} \int_0^\pi \zeta_\sigma(\Theta, \Phi) I[n\omega; E_0^{\text{eff}}(\Theta), \alpha(\Theta)] \\ &\quad \times \sin\Theta d\Theta d\Phi. \end{aligned} \quad (38)$$

(The interference phenomena between different benzene molecules in the sample are not taken into account.) The stability of the selection rules with respect to the degree of alignment is characterized by $\kappa_{5/3}$ and $\kappa_{7/9}$ which are defined by

$$\left. \frac{\bar{I}(5\omega)}{\bar{I}(3\omega)} \right|_{\kappa_{5/3}} = f, \quad \left. \frac{\bar{I}(7\omega)}{\bar{I}(9\omega)} \right|_{\kappa_{7/9}} = f. \quad (39)$$

The values of the maximum permissible alignments $\kappa_{5/3}$ and $\kappa_{7/9}$ are demonstrated for the range of intensities $22 \leq I_0 \leq 84 \text{ TW cm}^{-2}$ in Figs. 8(a) and 8(b). It can be concluded that the dynamical symmetry rules derived for circular polarized laser fields are feasible for significant deviations from circular polarization and/or from the perfect alignment of benzene.

VI. CONCLUSIONS

We have provided quantitative calculations of the selective HHG in aligned benzene molecule interacting with circular or nearly circular polarized laser field of 800 nm wavelength. Our results cover a wide range of the incident field intensities and offer a comprehensive picture of the strong field dynamics of the system. The use of the complex scaling technique in conjunction with Floquet theory allowed us to obtain the general solution of the time-dependent problem in

terms of a set of resonance quasi-energies and the respective wave functions. Our results show that up to the intensity of about 90 TW cm^{-2} , the photo-induced dynamics of the molecule is dominated by a single long-lived resonance. The investigation of the dependence of the system lifetime on the intensity of the incident field allows us to estimate the degree of molecular ionization induced by the adiabatic laser pulse and the saturation intensity. The maximum intensity for an efficient HHG by the short laser pulses is limited by the saturation intensity. For example, the saturation intensity for a pulse supporting 15 optical cycles is calculated within the adiabatic approximation to be 55 TW cm^{-2} .

The calculated HHG spectra of aligned benzene driven in circular polarized field obey the DS-based selection rules, namely the $(6n \pm 1)$ th harmonics of the incident laser frequency are emitted.¹⁸ The benzene HHG spectra are found to consist of a plateau followed by an abrupt cutoff, in similarity to the paradigm case of atomic interaction with low-frequency, high-intensity linear polarized field. However, unlike in the atomic case, the length of the molecular HHG plateau grows linearly with the incident field amplitude. The distinct behavior of the molecular system has its origin in the completely different mechanism of the generation of the high-order harmonics. While the bound–continuum transitions are of paramount importance for the HHG in atoms interacting with the linear polarized field, it is the transitions between the low-energy bound states which make the dominant contribution to the molecular HHG at circular polarization. The importance of the bound–bound transitions for the selective molecular HHG has been demonstrated by the comparison of the converged numerical results with those of a twelve-state bound model.

The efficient coupling of the molecular bound states are also responsible for the significant enhancements of the high-order harmonics at specific field intensities. As demonstrated by our numerical calculations, this exciting effect has its origin in the avoided crossings of the resonance states in the complex energy plane. The enhancements predicted here theoretically in the case of molecular HHG possess an experimentally observed atomic counterpart. It is the so-called “resonance enhancement” of atomic HHG due to the strong (resonant) coupling between the ground and a (ac Stark shifted) Rydberg state.³³

Finally, we have considered the effect of the deviations from either the perfect circular polarization of the field or from the exact alignment of the benzene molecule on the stability of the DS-based selection rules. It has been found that 5% deviations from the ideal polarization or interaction geometry leave the DS-allowed harmonics strongly dominant in the HHG spectra. Our extensive model calculations allow us to conclude that the selective HHG in a sample of oriented gas-phase benzene molecules is a well-pronounced, stable effect, the observation of which should not be beyond the present-day experimental capabilities.

ACKNOWLEDGMENTS

This work was supported in part by Aly Kaufmann fellowship, by U.S.-Israel Binational Science Foundation, by the Basic Research Foundation administered by the Israeli

Academy of Sciences and Humanities and by the Fund for the Promotion of Research at the Technion. The authors wish to acknowledge the Center for Complex Molecular Systems and Biomolecules, which is funded by the Czech Ministry of Education (Grant No. LN00A032), for providing their computing facilities to help to complete this study.

APPENDIX: TRANSITION DIPOLE MOMENT MATRIX ELEMENTS

The transition dipole moment matrices for the benzene electronic states, $\mathbf{M}_{\theta\pm}$, are calculated using the momentum matrices. From Eq. (11) one obtains immediately

$$\mathbf{M}_{\theta\pm} = \frac{E_0 e}{2m_e \omega} (\pm i \mathbf{P}_{\theta x} \cos \alpha + \mathbf{P}_{\theta y} \sin \alpha), \quad (\text{A1})$$

where the momentum matrices $\mathbf{P}_{\theta x}$ and $\mathbf{P}_{\theta y}$, represent the operators $\hat{p}_{\theta x}$ and $\hat{p}_{\theta y}$, respectively, in the basis set of $\{\Psi_{\theta}^{(0)}\}$. $\mathbf{P}_{\theta x,y}$ are given by unitary transformation of the "primitive" momentum matrices $\mathbf{P}_{\theta x,y}^{\chi}$

$$\mathbf{P}_{\theta x,y} = \mathbf{c}_{\theta}^{(0)T} \mathbf{P}_{\theta x,y}^{\chi} \mathbf{c}_{\theta}^{(0)}, \quad (\text{A2})$$

where matrix $\mathbf{c}_{\theta}^{(0)}$ contains the coefficients in the primitive basis set expansion of the electronic states of benzene

$$\Psi_{\theta,i}^{(0)} = \sum_{\{m,k\}} \chi_{m,k} c_{\theta\{m,k\},i}. \quad (\text{A3})$$

$\mathbf{P}_{\theta x,y}^{\chi}$ is the matrix representation of operators $\hat{p}_{\theta x,y}$ in terms of the primitive basis set $\{\chi_{m,k}\}$,

$$P_{\theta x,y\{m,k\},\{m',k'\}}^{\chi} = \langle \chi_{m,k} | \hat{p}_{\theta x,y} | \chi_{m',k'} \rangle. \quad (\text{A4})$$

It is convenient to define operators

$$\hat{p}_{\theta\pm} = -i\hbar e^{-i\theta} \frac{e^{\mp i\phi}}{2} \left(\frac{\partial}{\partial r} \mp \frac{i}{r} \frac{\partial}{\partial \phi} \right), \quad (\text{A5})$$

where the following relations hold:

$$\begin{aligned} \hat{p}_{\theta x} &= \hat{p}_{\theta+} + \hat{p}_{\theta-}, \\ \hat{p}_{\theta y} &= i(\hat{p}_{\theta+} - \hat{p}_{\theta-}). \end{aligned} \quad (\text{A6})$$

The matrix representation $\mathbf{P}_{\theta\pm}^{\chi}$ of $\hat{p}_{\theta\pm}$ is defined by

$$\begin{aligned} P_{\theta\pm\{m,k\},\{m',k'\}}^{\chi} &= \langle \chi_{m,k} | \hat{p}_{\theta\pm} | \chi_{m',k'} \rangle \\ &= \int_0^{2\pi} \int_0^{r_{\max}} \chi_{m,k}^* \hat{p}_{\theta\pm} \chi_{m',k'} r dr d\phi. \end{aligned} \quad (\text{A7})$$

We express the functions $\chi_{\{m,k\}}$ using Eq. (3) and obtain

$$\begin{aligned} P_{\theta\pm\{m,k\},\{m',k'\}}^{\chi} &= -i\hbar e^{-i\theta} \frac{N_{m,k} N_{m',k'}}{2\pi} \int d\phi dr r J_{|m|}(kr) \\ &\times e^{-im\phi} \frac{e^{\mp i\phi}}{2} \left(\frac{\partial}{\partial r} \mp \frac{i}{r} \frac{\partial}{\partial \phi} \right) \\ &\times [J_{|m'|}(k'r) e^{im'\phi}]. \end{aligned} \quad (\text{A8})$$

The working expression for $\mathbf{P}_{\theta\pm}^{\chi}$ obtained after a few algebraic manipulations reads

$$\begin{aligned} P_{\theta\pm\{m,k\},\{m',k'\}}^{\chi} &= \delta_{m'-m,\pm 1} \frac{-i\hbar e^{-i\theta}}{2} N_{m,k} N_{m',k'} \\ &\times \left[k' \int_0^{r_{\max}} dr r J_{|m|}(kr) J'_{|m'|}(k'r) \right. \\ &\left. \pm m' \int_0^{r_{\max}} dr J_{|m|}(kr) J_{|m'|}(k'r) \right]. \end{aligned} \quad (\text{A9})$$

The evaluation of Bessel function $J_m(z)$ and its derivative $J'_m(z)$ is performed using computational routines of Numerical Recipes.³⁷

¹Y. Liang, S. Augst, S. L. Chin, Y. Beaudoin, and M. Chaker, J. Phys. B **27**, 5119 (1994).

²H. Sakai and K. Miyazaki, J. Phys. B **61**, 493 (1995).

³C. Lyngå, A. L'Huillier, and C.-G. Wahlström, J. Phys. B **29**, 3293 (1996).

⁴Y. Liang, A. Talebpour, C. Y. Chien, S. Augst, and S. L. Chin, J. Phys. B **30**, 1369 (1997).

⁵P. B. Corkum, Phys. Rev. Lett. **71**, 1994 (1993).

⁶K. Kulander, K. Schafer, and J. Krause, in *Super-Intense Laser-Atom Physics, Vol. 316 of NATO Advanced Study Institutes, Series B: Physics*, edited by B. Piraux, A. L'Huillier and K. Rzażewski (Plenum, New York, 1993), p. 316.

⁷R. Numico, P. Moreno, L. Plaja, and L. Roso, J. Phys. B **31**, 4163 (1998).

⁸A. D. Bandrauk and H. Yu, J. Phys. B **31**, 4243 (1998).

⁹N. Hay, R. Velotta, M. B. Mason, M. Castillejo, and J. P. Marangos, J. Phys. B **35**, 1051 (2002).

¹⁰D. J. Fraser, M. H. R. Hutchinson, J. P. Marangos, Y. L. Shao, J. W. G. Tisch, and M. Castillejo, J. Phys. B **28**, L739 (1995).

¹¹N. Hay, M. Castillejo, R. de Nalda, E. Springate, K. J. Mendham, and J. P. Marangos, Phys. Rev. A **61**, 053810 (2000).

¹²N. Hay, R. de Nalda, T. Halfmann, K. J. Mendham, M. B. Mason, M. Castillejo, and J. P. Marangos, Phys. Rev. A **62**, 041803(R) (2000).

¹³N. Hay, R. de Nalda, T. Halfmann, K. J. Mendham, M. B. Mason, M. Castillejo, and J. P. Marangos, Eur. Phys. J. D **14**, 231 (2001).

¹⁴W. Kim and P. M. Felker, J. Chem. Phys. **104**, 1147 (1996); H. Sakai, C. P. Safvan, J. J. Larsen, K. M. Hilligsøe, K. Hald, and H. Stapelfeldt, *ibid.* **110**, 10235 (1999); J. J. Larsen, H. Sakai, C. P. Safvan, I. Wendt-Larsen and H. Stapelfeldt, *ibid.* **111**, 7774 (1999).

¹⁵R. Kopold, W. Becker, and M. Kleber, Phys. Rev. A **58**, 4022 (1998).

¹⁶D. G. Lapps and J. P. Marangos, J. Phys. B **33**, 4679 (2000).

¹⁷N. Hay, R. Velotta, M. Lein, R. de Nalda, E. Heesel, M. Castillejo, and J. P. Marangos, Phys. Rev. A **65**, 053805 (2002); R. Velotta, N. Hay, M. B. Mason, M. Castillejo, and J. P. Marangos, Phys. Rev. Lett. **87**, 183901 (2001).

¹⁸O. E. Alon, V. Averbukh, and N. Moiseyev, Phys. Rev. Lett. **80**, 3743 (1998).

¹⁹O. E. Alon, Phys. Rev. A **66**, 013414 (2002).

²⁰V. Averbukh, O. E. Alon, and N. Moiseyev, Phys. Rev. A **64**, 033411 (2001).

²¹M. Lewenstein, Ph. Balcoup, M. Yu. Ivanov, A. L'Huillier, and P. B. Corkum, Phys. Rev. A **49**, 2117 (1994); P. Antoine, A. L'Huillier, M. Lewenstein, P. Salières, and B. Carré, *ibid.* **53**, 1725 (1996).

²²M. Yu. Ivanov and P. B. Corkum, Phys. Rev. A **48**, 580 (1993).

²³J. L. Krause, K. J. Schafer, and K. C. Kulander, Phys. Rev. A **45**, 4998 (1992); Phys. Rev. Lett. **68**, 3535 (1992).

²⁴F. Ceccherini and D. Bauer, Phys. Rev. A **64**, 033423 (2001).

²⁵F. Ceccherini, D. Bauer, and F. Cornolti, J. Phys. B **34**, 5017 (2001).

²⁶M. L. Pons, R. Taïeb, and A. Maquet, Phys. Rev. A **54**, 3634 (1996).

²⁷W. P. Reinhardt, Annu. Rev. Phys. Chem. **33**, 223 (1982).

²⁸N. Moiseyev, Phys. Rep. **302**, 211 (1998).

²⁹U. Peskin and N. Moiseyev, J. Chem. Phys. **99**, 4590 (1993).

³⁰N. Ben-Tal, N. Moiseyev, R. Kosloff, and C. Cerjan, J. Phys. B **26**, 1445 (1993).

³¹N. Moiseyev and F. Weinhold, Phys. Rev. Lett. **78**, 2100 (1997).

³²T. Timberlake and L. E. Reichl, Phys. Rev. A **59**, 2886 (1999).

³³E. S. Toma, Ph. Antoine, A. de Bohan, and H. G. Muller, J. Phys. B **32**, 5843 (1999).

- ³⁴U. Peskin, O. E. Alon, and N. Moiseyev, *J. Chem. Phys.* **100**, 7310 (1994).
- ³⁵S. M. Hankin, D. M. Villeneuve, P. B. Corkum, and D. M. Rayner, *Phys. Rev. Lett.* **84**, 5082 (2000).
- ³⁶G. P. Agrawal, *Nonlinear Fiber Optics*, 2nd ed. (Academic, San Diego, 1995).
- ³⁷W. H. Press, S. A. Teukolsky, W. T. Vetterling, and B. P. Flannery, *Numerical Recipes in C: The Art of Scientific Computing*, 2nd ed. (Cambridge University Press, Cambridge, 1988–1992).
- ³⁸B. Sheehy, J. D. D. Martin, L. F. DiMauro, P. Agostini, K. J. Schafer, M. B. Gaarde, and K. C. Kulander, *Phys. Rev. Lett.* **83**, 5270 (1999).
- ³⁹V. R. Bhardwaj, D. M. Rayner, D. M. Villeneuve, and P. B. Corkum, *Phys. Rev. Lett.* **87**, 253003 (2001).